

Effect of Chain Chirality on the Self-Assembly of Sickle Hemoglobin

Xuejin Li,[†] Bruce Caswell,[‡] and George Em Karniadakis^{†*}

[†]Division of Applied Mathematics and [‡]School of Engineering, Brown University, Providence, Rhode Island

ABSTRACT We present simulation results on the self-assembly behavior of sickle hemoglobin (HbS). A coarse-grained HbS model, which contains hydrophilic and hydrophobic particles explicitly, is constructed to match the structural properties and physical description of HbS. The hydrophobic interactions are shown to be necessary with chirality being the main driver for the formation of HbS fibers. In the absence of chain chirality, only small self-assembled aggregates are observed whereas self-assembled elongated steplike bundle microstructures appear when we include chain chirality. We also investigate the effect of confinement on self-assembly, and find that elongated fibers—similar to open-space ones—can be obtained in hard confinement domains but cannot be formed within compliant red blood cell (RBC) domains under the same assumptions. We show, however, that by placing explicitly HbS fibers inside the RBCs and subjecting them to linear elongation and bending, we obtain different types of sickle-shaped RBCs as observed in sickle cell anemia.

INTRODUCTION

Self-assembly, which makes use of molecular rather than atomic units, offers a bottom-up approach to the development of complex materials at different length scales (1). The ability to self-assemble is inherent in biological macromolecules such as proteins and phospholipids but also in synthetic amphiphiles, i.e., surfactants and block copolymers. Recently, increased attention has been given to chiral molecular self-assembly (2) with chiral molecules lacking internal planes of symmetry. Chiral molecules are able to self-assemble into a variety of finite structures ranging from zero-dimensional spherical micelles to one-dimensional elongated micelles to extended two-dimensional sheetlike micelles (3). These chiral self-assembled structures are widely found in natural systems, such as twisted fibers, helical ribbons, and nanotubes.

Chiral molecular self-assembled structures have also been associated with a number of human diseases, including amyloid formation in neurodegenerative diseases such as Alzheimer's and Parkinson's (4), sickle cell anemia induced by the growth of polymer fibers (5), and gallstones formation in nucleating bile (6). In particular, sickle cell anemia has been characterized as the first “molecular disease” (7). The symptoms of the disease have been traced to the polymerization of sickle hemoglobin (HbS) at high enough concentrations, forming long fibers that distort the shape of red blood cells (RBCs) and dramatically alter their mechanical and rheological properties (8,9). Moreover, the sickle-shaped cells may adhere to the wall of small blood vessels, and hence brain perfusion can be affected. Damage of the affected organs, pain, and often death, are the main clinical manifestations of sickle cell anemia (10). The sequence of events in a sickle-cell crisis is: nucleation, polymerization,

cell deformation, and then vaso-occlusion, revealing that HbS polymerization is the primary cause of the clinical disease manifestations (11–13).

HbS polymerization is a dynamic event that can be modeled as a double nucleation mechanism (14–16). The three stages in the formation of HbS fibers are 1), homogeneous nucleation of polymer fibers, 2), fiber growth by the addition of HbS molecules, and 3), fiber branching by secondary nucleation of new fibers on top of existing ones. A different mechanism of polymerization has been suggested by recent experiments and theory (17–19). According to this mechanism, there are two steps in the formation of nucleation of HbS fibers: 1), the formation of dense liquid droplets, and 2), the formation of fiber nuclei within these droplets. Subsequently, HbS fibers grow spontaneously and interact continuously with the soft membrane of SS-RBCs, resulting in deformed shapes.

Due to the intriguing nonequilibrium nature of chiral self-assembly and self-assembled nanostructures, their fundamental understanding—especially one-dimensional chiral self-assembled structures such as twisted fibers and helical nanotubes—have important physical and biological implications. For example, Turner et al. (20) constructed a theoretical model for the thermodynamic stability and equilibrium pitch length of fibers, demonstrating that twist effects play an essential role in stabilizing HbS fibers. Dynamic simulations of self-assembled filamentous bundles by Yang et al. (21) confirm that chain chirality is the reason for self-limited bundle sizes, and that strong interactions lead to the formation of branched networks. Li and Lykotrafitis (22) developed a solvent-free coarse-grained molecular dynamics model to represent a single hemoglobin fiber as four tightly bonded chains, and they found their model could simulate the mechanical behavior of single HbS fibers. In recent work, Lei and Karniadakis (23) employed a validated multiscale model of RBCs to simulate the morphology and dynamic properties of sickle cells. In particular, they

Submitted March 8, 2012, and accepted for publication August 3, 2012.

*Correspondence: george_karniadakis@brown.edu

Editor: Nathan Baker.

© 2012 by the Biophysical Society
0006-3495/12/09/1130/11 \$2.00

<http://dx.doi.org/10.1016/j.bpj.2012.08.017>

quantified cell distortion with asphericity and elliptical shape factors, and their results are consistent with the medical image observations (24,25).

The kinetic and dynamic details of these processes remain largely unknown. Molecular-level simulation will help in understanding HbS polymerization; however, to the best of our knowledge, no particle-based model has been used to accurately describe the particular structure of HbS molecules nor the crowding effects on self-assembly at high density. In this study, we present a coarse-grained model of HbS, and use it to simulate the self-assembly behavior of HbS. Our interest lies in the effect of molecular chirality on the HbS self-assembly and in observing possible shape deformation of RBC induced by the growth of HbS fibers. We employ the dissipative particle dynamics (DPD) method, a coarse-grained particle-based simulation technique in three dimensions, which correctly represents hydrodynamic interactions (26). The rest of this work is organized as follows: We describe the mesoscopic HbS model and briefly describe the DPD simulation method. We then present and discuss the simulation results. The findings from the simulation studies and the model predictions are summarized in Conclusion, together with possible future applications of such a model.

MODEL AND SIMULATION METHOD

Mesoscopic model

Normal RBCs contain hemoglobin A composed of two α - and two β -subunits; the pairing of one of each of α and β produces a hemoglobin dimer. However, the hemoglobin dimer does not efficiently deliver oxygen. Two dimers combine to form a hemoglobin tetramer, the functional form of hemoglobin. As the RBCs traverse the microcirculation, oxygen is released from oxyhemoglobin to generate deoxyhemoglobin. Upon deoxygenation, the glutamic acid (Glu) in hemoglobin is replaced by the less-polar amino acid, valine (Val), at the sixth position of the β -subunit. The Glu-6(β) \rightarrow Val mutation in deoxy-HbS favors a hydrophobic interaction between each strand and its neighbor (27).

The abnormal hemoglobin in which valine replaces glutamic acid renders the hemoglobin less soluble under decreasing oxygen concentrations, and leads to polymerization into large fibers that distort the RBCs into sickle shapes. In this study, a coarse-grained model is constructed to match the physical description and structural properties of the HbS molecule. Specifically, one hemoglobin molecule is built with two hydrophilic particles (denoted by A) and two hydrophobic particles (denoted by B). Particles A and B are joined together by a harmonic spring to form a dimer. Two dimers are then connected by harmonic springs to form a tetramer, i.e., the HbS molecule (see Fig. 1 a).

With only four particles, the HbS model is admittedly too simple to represent all of the structural properties of an HbS molecule. In this study, however, our model is not intended to represent the formation of fiber nuclei, but instead, it focuses on the growth of HbS fibers. Thus, several HbS molecules are then connected by harmonic springs to form an HbS single strand (see Fig. 1 b). The symbol n in this figure represents the

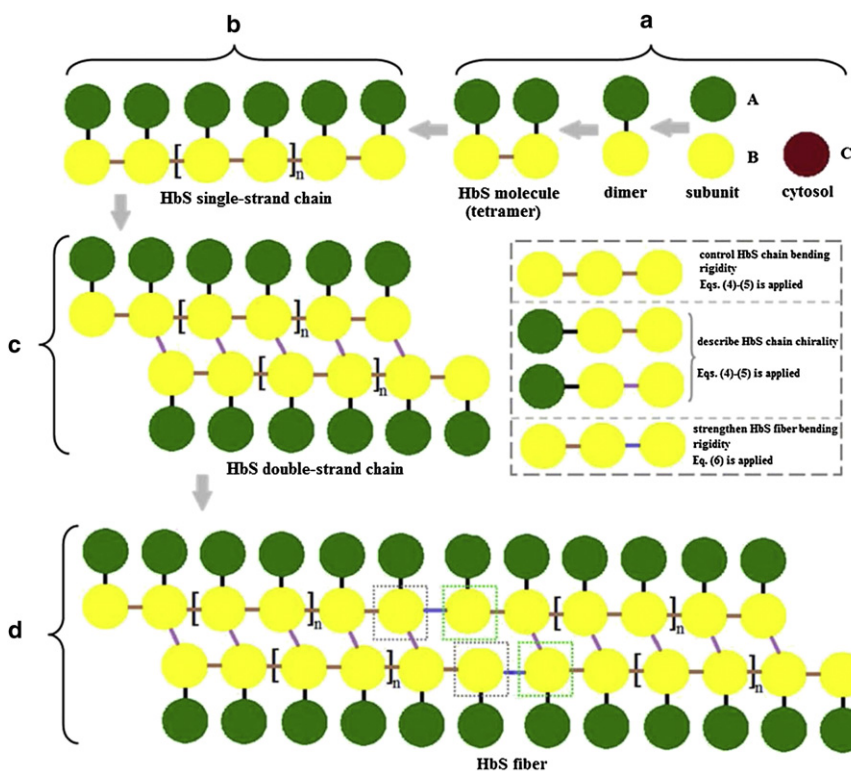


FIGURE 1 Schematic of the coarse-grained HbS model. The A and B particles represent the α - and β -subunits of HbS. All connections (A-A, B-B, and A-B) are harmonic springs. The HbS molecule is a tetramer formed by two A-B dimers (a). Several HbS molecules are then connected to form a HbS single strand (b). The symbol n is the number of internal repeat units in a HbS strand. Here the coarse-grained HbS model uses $n = 3$ with two end units; the HbS strand then consists of five molecules. In addition, one of the two B particles of a HbS molecule in one strand is then connected to another B particle of the partner strand to form a hydrophobic contact (c). The C particle represents the cytosol; a large number of cytosolic particles describe the crowding effects inside the RBC. The A and C particles are hydrophilic whereas the B particles are hydrophobic. (Sketch enclosed within the dashed line) Confinement effect of HbS chains. To impart the bending rigidity to HbS chain, the connections among three consecutive hydrophobic particles in the same HbS strand are constrained to a prescribed angle. Two types of bond-bending interactions are included to control the chirality of HbS chain, one of which is exerted between one hydrophilic particle and two consecutive hydrophobic particles in a same HbS strand, combined with the other exerted between the hydrophilic particle and two consecutive hydrophobic particles in two different HbS strands. A bond-bending force is added to those hydrophobic particles from two different HbS chains when their free ends (enclosed within the dotted line) have a close contact (d).

number of internal repeat HbS units. In this study, $n = 3$ is used for the coarse-grained HbS model, thus, five HbS molecules are linked together in one strand.

Upon deoxygenation, the replacement of a β -subunit at the site of $\beta 6$ with valine results in a hydrophobic interaction. Here, we take the B particles to be hydrophobic and the A particles to be hydrophilic. Experimental investigation also shows that the primary structural unit is a double strand in which HbS molecules are staggered (28). The hemoglobin tetramer is oriented in such a way that one of the two β -subunits forms a hydrophobic contact at the $\beta 6$ site with a complementary or acceptor site on a β -subunit of the partner strand. For this reason, this connection is made by harmonic springs, as also shown in Fig. 1 c. Cytosolic particles (denoted by C) are included explicitly to describe the crowding effect in the models; however, for clarity, they are not shown in the following figures, except later in Fig. 8.

Dissipative particle dynamics formulation

The self-assembly of HbS is simulated with dissipative particle dynamics (29). DPD describes clusters of molecules moving together in a Lagrangian fashion subject to soft repulsive potentials. In a DPD simulation, a particle represents the center of mass in a cluster of atoms, and the position and momentum of the particle is updated in a continuous phase at discrete time steps. Particles i and j at positions r_i and r_j interact with each other via pairwise conservative, dissipative, and random forces. Specifically, in our simulations we have

$$F_i = \sum_{i \neq j} \left(a_{ij} - \gamma \omega(r_{ij}) (\hat{r}_{ij} \cdot v_{ij}) + \sigma \zeta_{ij} / \sqrt{\delta t} \right) \omega(r_{ij}) \hat{r}_{ij}, \quad (1)$$

where a_{ij} is the maximum repulsion between particles i and j , and r_{ij} is the distance between them with the corresponding unit vector \hat{r}_{ij} . Also, v_{ij} is the difference between the two velocities, ζ_{ij} is a random number with zero mean and unit variance, and γ and σ are parameters coupled by $\sigma^2 = 2\gamma k_B T$, where k_B is the Boltzmann constant and T is the temperature. The weighting function $\omega(r_{ij})$ is given by

$$\omega(r_{ij}) = \begin{cases} 1 - r_{ij}/r_c & r_{ij} < r_c \\ 0 & r_{ij} \geq r_c. \end{cases} \quad (2)$$

In the DPD method, the dissipative force and the random force act as heat sink and source, respectively, and the combined effect of the two forces forms a thermostat, which conserves momentum and thus provides the correct description of hydrodynamics for the system. Also, a common choice of the soft repulsion for the conservative force permits us to use larger integration time steps than are usually allowed in molecular dynamics. Thus, DPD is a simple but very effective simulation method that represents hydrodynamic interactions correctly.

The total force can also have an elastic contribution, which is derived from the harmonic force used to connect two consecutive particles in the HbS chains. The harmonic spring force with a spring constant of k_s and an equilibrium bond length of r_s in our simulations has the form

$$F_{ij}^S = -k_s (r_{ij} - r_s) \hat{r}_{ij}. \quad (3)$$

To control the HbS chain flexibility, an extra bond-bending force among three subsequent hydrophobic particles is added,

$$F^\theta = -\nabla V_{bend}, \quad (4)$$

$$V_{bend} = \frac{1}{2} k_\theta (\theta - \theta_0)^2, \quad (5)$$

where k_θ and θ_0 are the bond-bending constant and the equilibrium angle, respectively.

According to Yang et al. (21), chain chirality is the reason for self-limited, self-assembled bundle sizes; thus, we need to also consider chiral interactions. We then include a tunable bending-resistance interaction described by a bending finitely extensible-nonlinear-elastic force (30,31), which has the form

$$F_{bend} = k_{bend} \left[\frac{\theta - \theta_0}{1 - (\theta - \theta_0) / \Delta\theta_{max}} \right], \quad (6)$$

where $\Delta\theta_{max} = 0.3\theta_0$ is the maximum allowable bending angle between these hydrophobic particles. To simulate the self-assembly of HbS with chain chirality, the connections between two consecutive hydrophobic particles and one hydrophilic particle are constrained to a certain angle, θ_{ABB} . Specifically, two different types of bond-bending interactions are included to control the chirality of HbS chain, one of which is exerted between one hydrophilic particle and two consecutive hydrophobic particles in the HbS strand. It is applied in both directions with an equilibrium angle of $\theta_{ABB} \approx 90^\circ$; the other is exerted between one hydrophilic particle and two consecutive hydrophobic particles in two different HbS strands, with θ_{ABB} ranging from $0^\circ \sim 180^\circ$.

Moreover, an additional finitely extensible-nonlinear-elastic force, which is applied among three hydrophobic particles from two different HbS chains when the distance between their ends is less than a target distance, is also included to strengthen the bending rigidity of self-assembled HbS fibers. In this study, the bending rigidity of a HbS chain is mainly determined by the bond-bending force between hydrophobic particles, which are directed longitudinally along the fibrillar axis. The chiral interaction, which is lateral to the fibrillar axis, has only a slight influence on it. The nonbonded interactions are represented by pairwise additive forces. Specifically, these interaction terms are described by the conservative DPD forces.

Model parameters

Based on previous computational studies (32,33), the repulsive parameter related to the interaction between two like DPD particles is set at $a_{ii} = 25.00$ ($i = A, B, C$), causing the simulated compressibility of these DPD particles at room temperature to correspond to the experimental value. As suggested by Laradji and Sunil Kumar (34), the hydrophobic and hydrophilic interactions emerge from the relative interaction strengths a_{ij} . With this, the value of the parameter between two particles, one of which is hydrophilic and the other hydrophobic, is $a_{AB} = 50.0$, which is considered to be a sufficiently large value for the strong segregation (35). To model the amphiphilic nature of HbS, the repulsion parameter between the hydrophilic A- and cytosolic C-particles is made smaller than the repulsion parameter between two alike particles, i.e., $a_{AC} = 12.5$. Likewise, the parameter related to the interaction between the hydrophobic B- and cytosolic C-particles is made larger than the repulsion parameter between two similar particles, which ensures that the hydrophobic segment of HbS is sufficiently shielded from the cytosol. In this study, we choose $a_{BC} = 200.0$.

We then simulate a HbS single-strand chain in cytosol and employ the static scaling exponent (ν) in polymer solution to differentiate between hydrophilicity and hydrophobicity of DPD particles. As we just expect to differentiate the hydrophilicity and hydrophobicity of DPD particles, for the sake of simplicity, we assume a_{AC} and a_{BC} to be equal, and the HbS chain can be treated as a homopolymer chain. Following Kong et al. (36), the variation of repulsive parameter between HbS chain and solvent particles, a_{ij} , can be controlled by a solvent quality parameter, ϵ , which has the form $a_{ij} = a_{ii} (1 + \epsilon)$. When $\epsilon < 0$, the repulsion between the HbS chain and cytosol particles is weaker than that between two alike particles, leading to preferential association between these two particles and resulting in a hydrophilic interaction. When $\epsilon > 0$, the repulsion between

the HbS chain and cytosol particles is strong, leading to preferential separation between two particles and resulting in a hydrophobic interaction.

We then systematically vary the values of ϵ (a_{ij} changes simultaneously according to the above equation) and examine the static scaling exponent, ν , for a series of systems. Fig. 2 shows the scaling exponent as a function of DPD repulsive parameter for an HbS chain. We find that a parameter choice of $a_{ij} < 25.00$ leads to static scaling exponent ν of 0.58–0.61 for the radius of gyration with HbS chain length. These values are consistent with the value $a_{ij} \approx 0.59$, which characterizes the statistics of an excluded volume chain. We also find that $\nu = 0.30$ –0.32 for $a_{ij} > 28.50$, which agrees with the theoretical value of $\nu = 1/3$ for a collapsed polymer chain. In addition, the Flory-Huggins χN parameter is used to characterize the weak- and strong-segregation regimes. In general, we expect that $\chi N \gg 10.0$ for a strong-segregation regime whereas χN is ~ 10.0 for weak-segregation regime (37). In this study, $\chi N \approx 115$ for $a_{BC} = 100.0$ and $\chi N \approx 268$ for $a_{BC} = 200.0$, which puts us well outside the weak-segregation limit. Thus, the simulation results we present here do not change qualitatively by changing the repulsive parameter of a_{AC} in the range from 0.0 to 25.0 and a_{BC} in the range from 100.0 to 200.0.

Regarding the elastic contribution to the interaction energy, the spring constant is given by $k_s = 1000.0$ and the equilibrium bond length $r_s = 0.70r_c$. The hydrophobic segments of HbS are considered fairly rigid in our study; therefore the value of the equilibrium angle in these parts is set to $\theta_{ABB} = 180^\circ$. To determine the bending constant, k_θ , for the HbS chain, we require that the angular distribution of rigid parts be within our statistical accuracy. A value of $k_\theta = 200.0$ is found to satisfy this requirement. When the extra bond-bending force is introduced to the system, the rigidity of the hydrophobic part leads to an approximately constant length of long HbS chain. The end-to-end vector, which is the vector that points from one end of a polymer to the other end, can be used to describe the structural characteristics of polymer chain.

In this study, we measure the root mean-square end-to-end distance, $(\langle R^2 \rangle)^{0.5}$, from one free end to the other free end of a HbS double-strand chain. The normalized distribution of root mean-square end-to-end distance that is directed longitudinally along the fibrous axis for HbS chain with and without bond-bending forces is plotted in Fig. 3 a. In the absence of bond-bending force, a broad peak distribution is observed, and the values of the main peak are distributed in the range from $1.3r_c$ to $2.1r_c$, where r_c is the cutoff radius in DPD simulations. In the presence of bond-bending force, the distribution of root mean-square end-to-end distance along the fibrous axis turns into a sharp one and the peak shifts toward a value of $4.0r_c$, which is higher than that of fully flexible chains (without the bond-bending force). Next, we calculate the angle, ϕ , between the vectors from the center of mass of the whole HbS molecular backbone to the centers of mass of each side along the fibrous axis, and investigate the angular distribution, $P(\phi)$, in HbS chains with and without bond-bending forces. It had been previously proposed that the following equation be used to calculate the $\cos\phi$ (38),

$$\cos\phi = \frac{(\mathbf{r}_{B1} - \mathbf{r}_B) \cdot (\mathbf{r}_{B2} - \mathbf{r}_B)}{|\mathbf{r}_{B1} - \mathbf{r}_B| |\mathbf{r}_{B2} - \mathbf{r}_B|}, \quad (7)$$

where \mathbf{r}_{B1} , \mathbf{r}_B , and \mathbf{r}_{B2} are the position vectors of the centers of mass of the first side, the HbS molecular backbone, and the second side, respectively. Fig. 3 b shows two representative results of $P(\phi)$ for HbS chains. Without considering the bond-bending force, we find that the angle can take a wide variety of values, whereas in the presence of bond-bending force, the distribution shows an obvious increase at $\phi > 120^\circ$ and a peak near $\phi > 160^\circ$, indicating that there hardly exist any folded chains. It is clear that the existence of the bond-bending force leads to the increase in individual HbS chain sizes, owing to the rigidity of the hydrophobic segments. Table 1 summarizes the parameters of interactions in the DPD simulations.

We use 8000 constituent particles of HbS molecules (2000 repeat units) with a homogeneous distribution in a simulation box of $30r_c \times 30r_c \times 30r_c$ with a particle number density of 3. Therefore, the total number of DPD particles in the system is 81,000. After these parameters are selected, the self-assembly aggregation of the HbS chains can be solely determined by the molecular chirality. Next, we present results from simulations of HbS systems. By changing θ_0 between the two consecutive hydrophobic B particles and one hydrophilic A particle, these HbS chains can self-assemble into complex microstructures, such as elongated sheetlike membrane and steplike HbS fibers. In these DPD simulations, the value of the number of HbS molecules in a HbS strand is fixed at 5. If the length of these HbS chains is too short, the HbS molecules cannot self-assemble into elongated sheetlike membrane or steplike HbS fibers. On the other hand, if the length of these HbS chains is too long, it is easier to form steplike HbS fibers but the size of the simulation box must also be larger to prevent periodic artifacts.

RESULTS AND DISCUSSION

The polymerization of HbS is a remarkably dynamic event. Study of the kinetics of HbS polymer formation, both in pure HbS solutions and in sickle erythrocytes, could provide insights into the pathogenesis of vaso-occlusive crises. We first run the three-dimensional DPD simulation in a periodic box. Without chiral interaction between hydrophobic B and hydrophilic A particles, only small size HbS aggregates are observed in the DPD simulations (see Fig. 4 a). One possible reason for this is that the hydrophilic particles can rotate freely; the coverage of hydrophilic particles on the surface of hydrophobic particles prevents direct connections between the hydrophobic and cytosolic particles.

When we consider the chain chirality, the stepped, elongated sheetlike membranes are observed from the DPD simulations (see Fig. 4 b). In this case, we choose the bending constant $k_{bend} = 200.0$ and equilibrium angle $\theta_{ABB} = 180.0^\circ$ with the maximum allowed bending angle $\Delta\theta_{max} = 0.1\theta_{ABB}$. The formation of this microstructure is a result of the local packing constraint between hydrophilic and hydrophobic particles due to strong chiral interaction. Two consecutive particles (one of which is hydrophilic and the other hydrophobic) on one strand are approximately colinear with another two consecutive particles on another strand; thus, the HbS chains pack parallel to each other into monolayer membrane to reduce the system's energy.

By decreasing the chiral interaction, i.e., the equilibrium angle decreases to $\theta_{ABB} = 120.0^\circ$ whereas the maximum allowed bending angle increases to $\Delta\theta_{max} = 0.3\theta_{ABB}$,

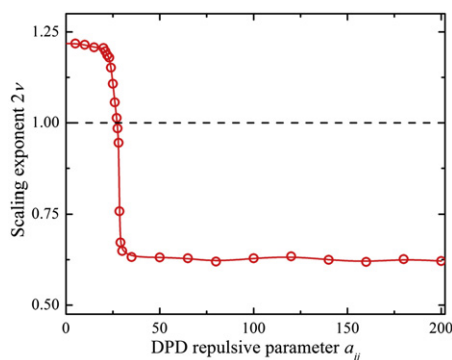


FIGURE 2 Scaling exponent, 2ν , as a function of DPD repulsive parameter, a_{ij} , for HbS chains.

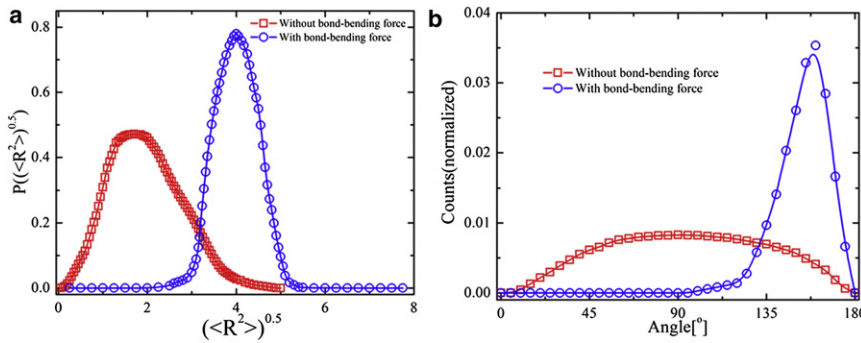


FIGURE 3 Normalized distribution of root mean-square end-to-end distance $\langle R^2 \rangle^{0.5}$ (a), and angular distribution of $P(\phi)$ (b) for HbS chains with and without bond-bending forces. In this figure, ϕ is the angle between the vectors from the center of mass of the HbS molecular backbone to the centers of mass of each side of HbS chains.

elongated steplike HbS fibers are obtained from the DPD simulations (see Fig. 5, left). In this case, the hydrophilic particles are still restricted due to the chain chirality. The hydrophobic particles have to pack more densely to form cylindrical microstructures to minimize contact with the cytosolic particles, resulting in the aggregation of HbS and persistent growth along one dimension to form elongated fibers (see Fig. 5, left). Some elongated HbS fibers are subsequently attracted and interact with the neighboring HbS fibers to form complex cross-linking network microstructures (see Fig. 4 c). However, without chiral interaction, the HbS chains cannot self-assemble into complex networklike structure, even if we use a much stronger bending rigidity. Thus, chirality is the main driver for the formation of HbS fibers.

The formation of polymer fibers is the primary cause of the characteristically deformed sickle RBCs. To quantify the shape of the self-assembled elongated fibers, we use the radius of gyration tensor (39) given by

$$S_{\gamma\delta}^2 = \frac{1}{MN} \sum (\gamma_i - \gamma_{cm})(\delta_i - \delta_{cm}), \quad (8)$$

where γ and δ are the x , y , and z coordinates of a particle, and γ_{cm} and δ_{cm} are the x , y , and z coordinates of the center-of-mass. Following Horsch et al. (40), we calculate the eigenvalues of the tensor and plot the three principal radii of gyration R_1 , R_2 , and R_3 ($R_1 \geq R_2 \geq R_3$). Fig. 5 (right) shows the radii of gyration for polymer fibers. Two of the principal radii, R_2 and R_3 , appear to be independent of the polymer fiber size over a broad range of sizes, whereas the third radius, R_1 , increases with the size of the polymer fiber.

It has been demonstrated that confinement has an influence on the self-assembly morphologies of biopolymers or soft matter (41). The polymerization of HbS fibers takes place within the RBC membrane, which is one type of a confined system. To illustrate the effect of the confinement on microstructure formation, we then simulate the self-assembly of HbS in bounded domains. In the DPD simulations, the confinement of HbS is realized by placing HbS inside a cube confined in two or three dimensions.

To start, we simulate the self-assembly of HbS under hard confinement, in which the shape of the bounded box is fixed

a priori and cannot be changed by the variation of either the internal self-assembled morphology or external conditions. From the DPD simulations, we find that the elongated steplike fibers and/or network microstructures can self-assemble from the HbS molecules (see Fig. 6). The type of the bounding domain may affect the self-assembly morphologies, and one can draw the phase diagram to show the difference from the self-assembly in bulk (42,43). Here, we also want to observe the possible effect of the aspect ratio of the geometry on the HbS self-assembly. To this end, we put the HbS molecules in a three-dimensional prism of $48r_c \times 48r_c \times 12r_c$ with three-dimensional confinement of which one dimension (z axis) is strongly confined. The confinement behavior is more pronounced in the strong confinement direction imposed by the asymmetric geometry; however, elongated fibers can be also formed from the HbS molecules (see Fig. 7, a and b).

Next, we study the growth of HbS residing inside a RBC, and observe possible shape deformation of the RBC induced by the HbS fibers. In this study, the RBC was simulated by a multiscale RBC model, which was developed by Fedosov et al. (44). In this model, the membrane of RBC is modeled by a two-dimensional triangulated network with $N_v = 9128$

TABLE 1 The interaction parameters in the DPD simulation

Interaction	Parameter			
Bond force		k_s	r_0	
	A-B	1000.0	0.70	
	B-B	1000.0	0.70	
Bond-bending force		k_0 (k_{bend})	θ_0	
	A-B-B*	200.0	90°	
	A-B-B†	200.0	0° ~ 180°	
	B-B-B‡	200.0	180°	
	B-B-B§	100.0	180°	
Repulsive force		A	B	S
	A	25.0	100.0	12.5
	B	100.0	25.0	200.0
	C	12.5	200.0	25.0

*For two consecutive B particles in the same HbS strand.

†For two consecutive B particles in two different HbS strands.

‡For three consecutive B particles in the same HbS strand.

§For two of three consecutive B particles in two different HbS chains.

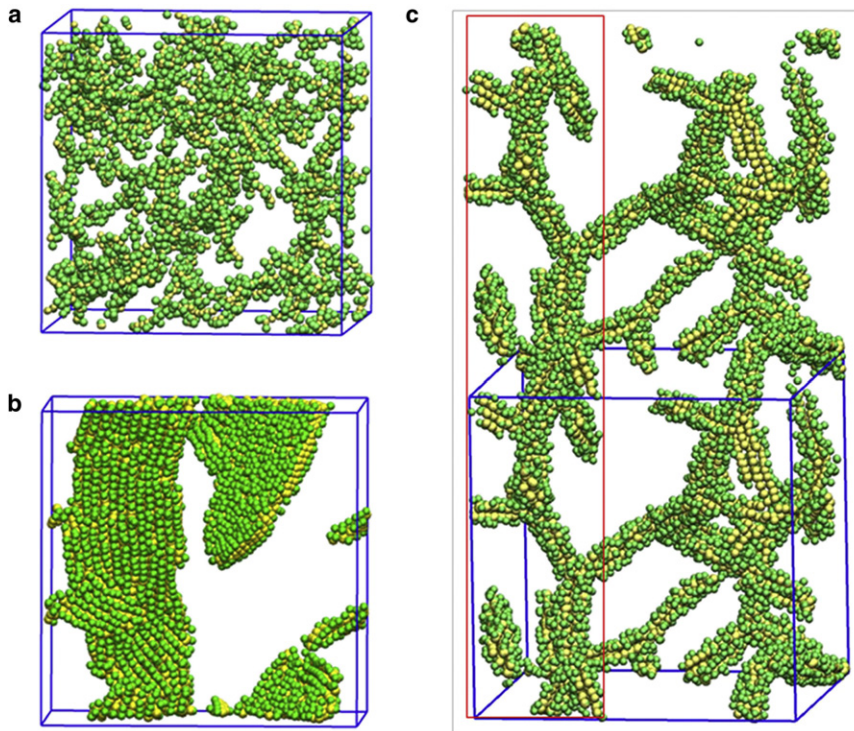


FIGURE 4 Self-assembled microstructures of HbS from the DPD simulations. Without chiral interaction between hydrophobic and hydrophilic particles, only small self-assembled aggregates (a) are observed. When chain chirality is included, self-assembled elongated sheetlike (b) and network (c) complex microstructures are obtained from the DPD simulations.

vertices, where each vertex is represented by a DPD particle. The vertices are connected by N_s viscoelastic bonds to impose proper membrane mechanics. The mechanical properties of the modeled membrane are fully determined by the experimentally established RBC macroscopic properties such that various cell membrane mechanical states can be imposed without any adjustment of parameters. The RBC linear and nonlinear elastic deformations match those obtained in optical-tweezers experiments (45,46). The rheological properties of the membrane have also been compared with those obtained in optical magnetic twisting cytometry, membrane thermal fluctuations, and creep followed by cell recovery (47). For details on the RBC model, we refer to Fedosov et al. (44) and Pivkin and Karniadakis (48).

We first simulate the HbS self-assembly in a rigid RBC by freezing the RBC membrane vertices, and we find that the HbS molecules can also self-assemble into elongated fibers

in this hard confinement (see Fig. 7, c and d). However, several of the elongated fibers buckle to conform with the RBC membrane curvature near the boundary. In our simulations, the RBC is rigid and its shape cannot be deformed, thus, it is expected that the shape of the RBC cross section affect the HbS self-assembly. In biological systems such as RBCs, self-assembly takes place in a confined environment whose boundary is not rigid but compliant. The self-assembled microstructure under this soft confinement should be different because of the flexibility of the confined boundaries. In a recent study, Chi et al. (49) simulated the soft confinement-induced morphologies of diblock copolymers, in which they employed a “bad solvent” condition to describe the soft confinement effect. To the best of our knowledge, this is the only work related to the soft-confinement-induced self-assembly using particle-based molecular simulations.

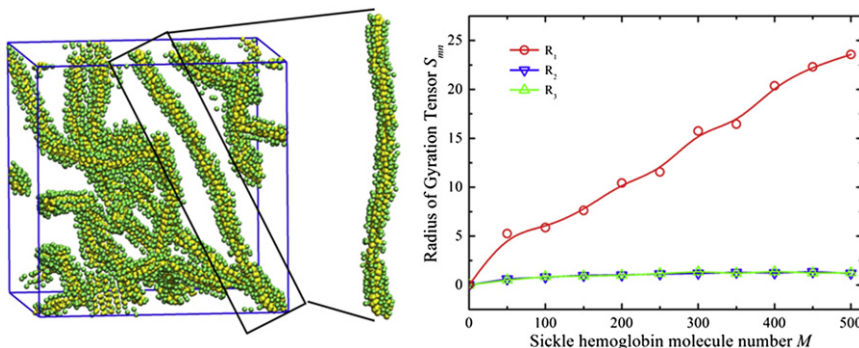


FIGURE 5 (Left) Self-assembled elongated steplike fibers at $\theta_{ABB} \approx 120.0^\circ$. (Right) Radius of representative gyration tensor as a function of the number of sickle hemoglobin molecules. In this figure, ϕ represents the number of sickle hemoglobin molecules in an individual self-assembled HbS fiber.

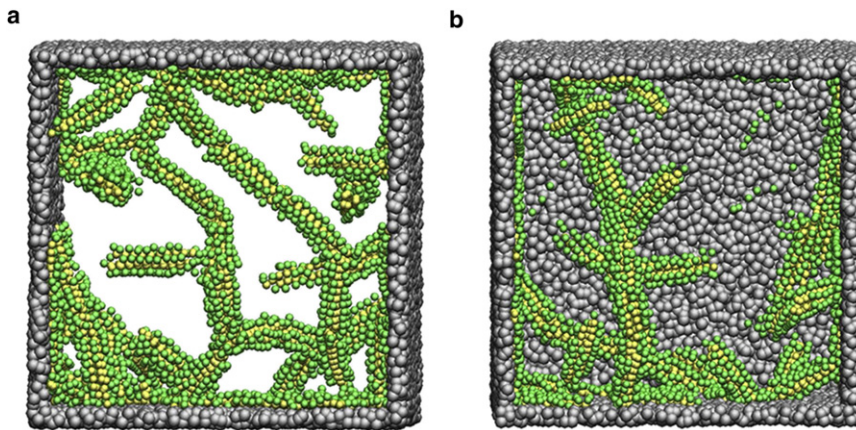


FIGURE 6 Self-assembled microstructures of HbS molecules from the DPD simulations in a cube $30r_c \times 30r_c \times 30r_c$ with two-dimensional confinement (a) and three-dimensional confinement (b). In this figure, the gray particles represent the wall particles. For clarity, the front wall particles are not shown in panel b.

In Fig. 8, we show the response of RBC obtained due to the aggregation of HbS molecules. In this soft confinement, the RBC can keep its shape when only the cytosolic particles are included inside the RBC membrane. Strong RBC membrane fluctuations take place when we include the HbS molecules into the RBC. To provide a more quantitative insight into the thermal fluctuation of the RBC membrane with and without HbS molecules, we computed the membrane fluctuation distributions for these two different cases following Fedosov et al. (47) (see Fig. 9). The RBC membrane with HbS molecules has a wider distribution, indicating that the shape of the RBC membrane is deformable with the internal self-assembled morphology. It is very difficult to study the self-assembly of HbS molecules under the soft confinement due to the moving and elastic boundaries of RBC. Moreover, for a strongly fluctuating RBC membrane the impenetrability between membrane and HbS molecules becomes important and leads to strong repulsive interactions

between them, which also affect the self-assembly of HbS molecules. Hence, in our simulations we find that the HbS molecules cannot self-assemble into elongated HbS fiber inside a compliant RBC under conditions and parameters similar to the ones employed in the open-space and hard-confinement simulations. This may be related to the RBC membrane model employed in this study and it will be investigated in future work more systematically.

Here to circumvent this difficulty, we can start the simulation by placing an elongated HbS fiber (already formed in the three-dimensional periodic system) inside the RBC, and use a linear spring model to simulate the growth of the HbS fiber. This has the form (50)

$$F_{ij}^S = k_s [l_{ref}(p_{O_2}) - l], \quad (9)$$

where l is the curvilinear length of the HbS fiber, and l_{ref} is the expected length of the HbS fiber for a given oxygen

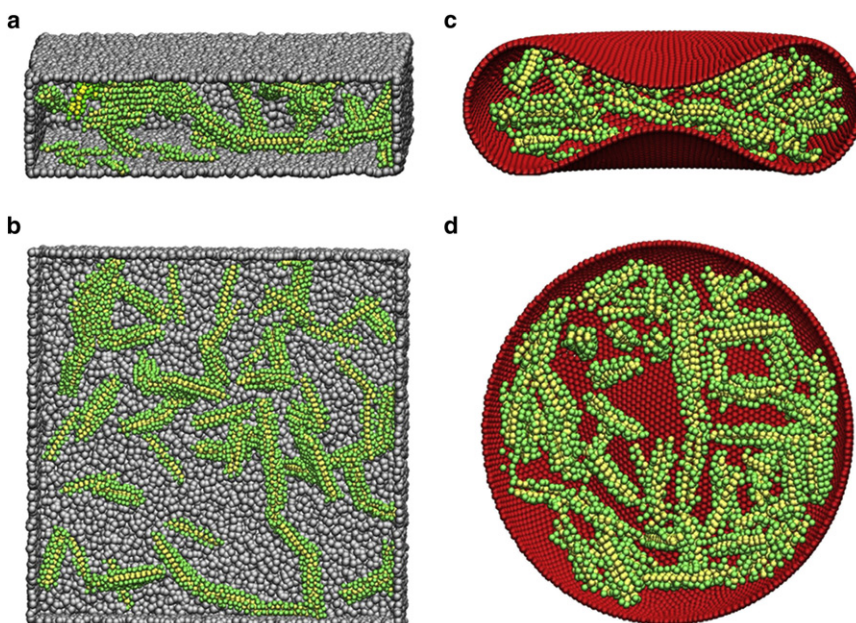


FIGURE 7 Self-assembled microstructures of HbS molecules from the DPD simulations in a prism of $48r_c \times 48r_c \times 12r_c$ with three-dimensional confinement (a and b) and inside a rigid RBC by freezing the RBC membrane vertices. (Shaded particles) Wall particles. For clarity, the front wall particles are not shown in panels a and b, and only half of the RBC membrane is shown in panels c and d. Panels a and c show the views of the simulation results while panels b and d show vertical views of the simulation results.

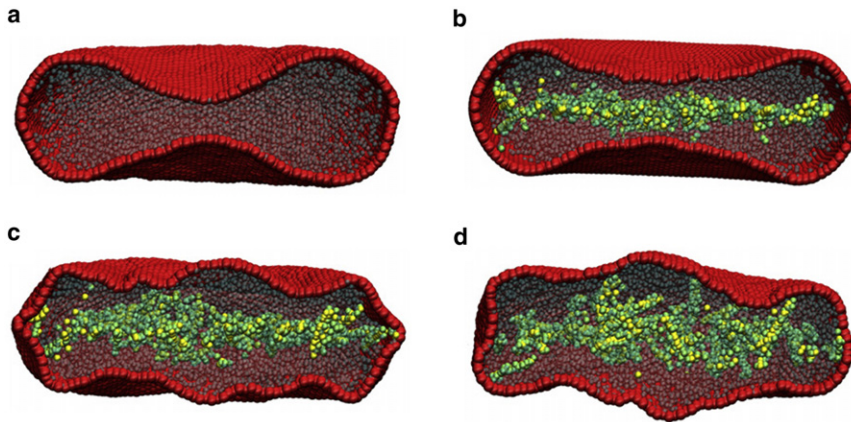


FIGURE 8 RBC responses obtained for only cytosolic particles included inside the RBC membrane (a); and sickle hemoglobin molecules and cytosolic particles included inside the RBC membrane at the initial state (b), intermediate state (c), and metastable state (d).

concentration. It had been previously proposed that the following equation be used to describe the $l_{ref}(p_{O_2})$ (50),

$$l_{ref}(p_{O_2}) = l_0 \left\{ 1 - \left[\left(\frac{l_{ref}}{l_0} \right)_{max} - 1 \right] \left[\frac{p_{O_2-ref} - p_{O_2}}{p_{O_2-ref}} \right] \right\}, \quad (10)$$

where l_0 is the reference HbS length before sickling, corresponding to oxygen partial pressure p_{O_2-ref} , and

$$\left(\frac{l_{ref}}{l_0} \right)_{max}$$

is the maximum relative elongation of the HbS with respect to the reference state.

In contrast to normal RBCs, sickle cells exhibit various morphological states due to the polymerization of HbS and alignment of fibers inside the RBC. In the deoxygenated state, the HbS molecules aggregate and persistently grow along one dimension to form elongated fibers. Consequently, the RBC undergoes various degrees of distortion due to the interaction between the growing HbS fibers and the RBC membrane. Indeed, when we increase the length of the HbS fiber, we find the HbS can deform the RBC shape, and become sickle-shaped cell (see Fig. 10). If we put a cross-linking microstructure inside the RBC, and use a similar method, we find that the RBC become a holly leaf-shaped cell (see Fig. 11). Different self-assembled microstructures from HbS molecules have been observed in experiments. The polymerization of HbS is the primary cause of the sickle cell disease, while the alignment of these self-assembled HbS fibers distorts RBC membranes and deforms their shapes. So, the sickle RBC shapes also depend on the number of the HbS fibers, which is related to the deoxyhemoglobin concentration values and the rate of the deoxygenation procedure. In this study, we only focus on the effect of chain chirality on the self-assembly of HbS and the shape transformation of RBC induced by the growth of HbS fibers.

Following Lei and Karniadakis (23), we employ the asphericity shape factor (ASF) and elliptical shape factor (ESF) to quantify the RBC membrane distortion. The ASF and ESF, which are calculated from the eigenvalues of the radius of gyration tensor defined in Eq. 8, measure the deviation of the RBC from a spherical shape and the degree of the distortion on the x - y plane, respectively. From our simulations, we can compute

$$ASF = \frac{(R_1 - R_2)^2 + (R_2 - R_3)^2 + (R_3 - R_1)^2}{2(R_1 + R_2 + R_3)^2}, \quad (11)$$

$$ESF = \frac{R_1}{R_2}. \quad (12)$$

Table 2 shows the ASF and ESF for these two different types of sickle RBCs. Compared to the holly leaf-shaped RBC, the sickle-shaped RBC exhibits a larger distortion on the x - y plane and a smaller deviation from the healthy RBC.

In a recent study, Lei and Karniadakis (51) investigated the effect of HbS fiber length and cross-linking on the morphology of sickle RBCs using coarse-grained models of intracellular aligned hemoglobin polymers. They found

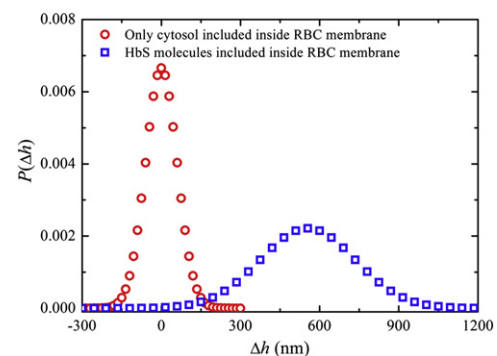


FIGURE 9 Thermal fluctuation distributions of RBC membrane with (squares) and without (circles) HbS molecules showing the increased fluctuation amplitudes due to HbS molecules.

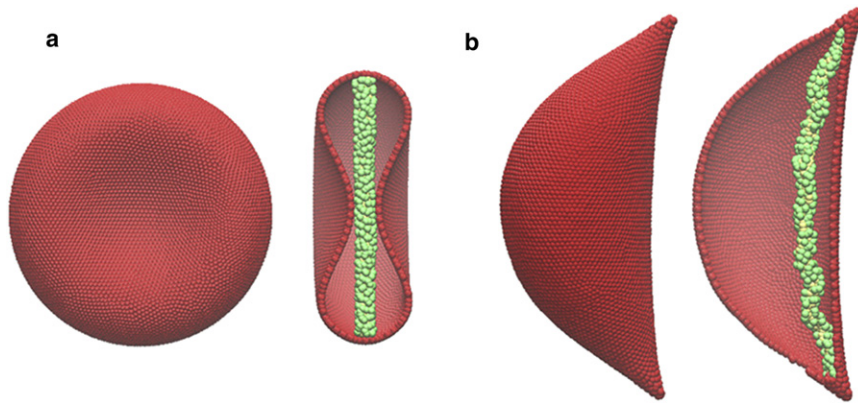


FIGURE 10 Sickle-shaped RBC induced by the growth of HbS fiber in DPD simulation. (a) The initial state of RBC and its slice; (b) the deformed sickle-shaped RBC and its slice.

that the final shape of sickle RBCs was determined by the angular width of the aligned hemoglobin polymer domain and the polymer growth rate as well as the cell membrane rigidity. In their study, the growth of the aligned hemoglobin polymer is modeled by adding single DPD particles to its end. Here we use a linear spring model to simulate the growth of the HbS fiber through continuous increase of the spring's equilibrium length to a specified length at a given oxygen concentration. The different RBC shapes we simulated in this study show consistent agreement with the simulation results of Lei and Karniadakis (51) and the experimental observations of Asakura et al. (25).

CONCLUSION

In this article, we have studied the self-assembled complex microstructures of sickle hemoglobin (HbS) and observed the shape deformation of red blood cell (RBC) induced by the growth of HbS fibers in dissipative particle dynamics (DPD) simulations. A coarse-grained HbS model has been developed to capture the structural properties of HbS and a large number of cytosolic particles describe the crowding effects inside the living cell. Specifically, one hemoglobin molecule was built with two hydrophilic and two hydrophobic particles, and the coarse-grained HbS model was constructed with several HbS molecules by joining consecutively hydrophobic particles with harmonic springs, forming a strand. In addition, one of the two hydrophobic particle

in a HbS molecule on one strand was connected to another hydrophobic particle in a neighboring HbS molecule on another strand to describe the hydrophobic patch between two different β -subunits.

The hydrophobic interactions were demonstrated to be necessary with chirality being the main driver for the formation of HbS fibers. Along with the introduction of an extra chiral interaction among three consecutive hydrophobic particles, the self-assembled microstructures and corresponding properties were anticipated to change significantly. In the absence of chain chirality, only small self-assembled aggregates were observed whereas self-assembled elongated steplike bundle microstructures appeared when we considered the chain chirality. We noted that the formation of these microstructures is a result of the local packing constraint due to chiral interactions.

We also investigated the response of a RBC due to the aggregation of HbS molecules. The RBC kept its shape when only the cytosolic particles were included inside the RBC membrane. Strong RBC membrane fluctuations took place when we included the HbS molecules into the RBC. The strong membrane fluctuations of RBC also affected the self-assembly of HbS molecules by suppressing the self-assembly process. To solve this problem, we need to further advance the multiscale RBC model and develop more appropriate membrane boundary conditions.

In this study, we placed an elongated HbS fiber (already formed in a three-dimensional periodic system) inside the

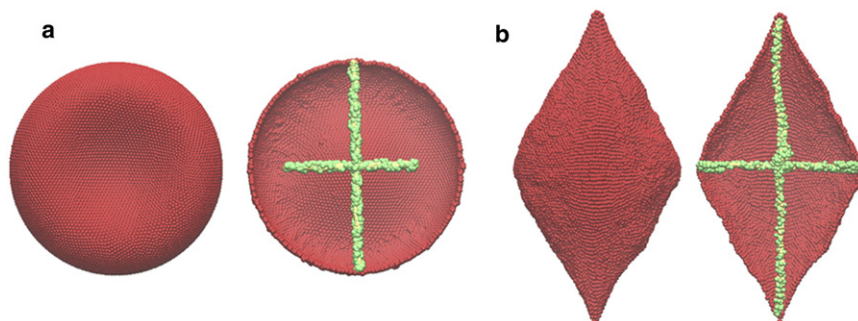


FIGURE 11 Holly leaf-shaped RBC induced by the growth of HbS fibers in DPD simulation. (a) The initial state of RBC and its slice; (b) the deformed holly leaf-shaped RBC and its slice.

TABLE 2 Computed ASF and ESF values for different RBC shapes

	Healthy RBC	Sickle-shaped RBC	Holly leaf-shaped RBC
ASF	0.274	0.578	0.812
ESF	1.000	2.917	1.854

RBC, and used a linear spring model to simulate the growth of the HbS fiber. The linear elongation and bond-bending interactions of HbS fibers led to sickle-shaped cells. These findings demonstrate that the DPD method is an effective (relatively simple) simulation technique for understanding the dynamics of self-assembly HbS fibers as well as the RBC responses to the polymerization and gelation of HbS, but further work is required to accurately model the intriguing fiber-membrane interactions.

Using this new, to our knowledge, comprehensive multi-scale model, it would be possible to study the influence of fetal hemoglobin (HbF) in conjunction with HbS. The pathophysiology of sickle cell disease is dependent on the polymerization of HbS. The replacement of one β -subunit of HbS by a γ -subunit appears to have a strong inhibitory effect on HbS polymerization (52). However, HbS gelation studies show that HbF does not interact with HbS: the HbF dissociates to a dimer ($\alpha_1\gamma_1$), which can be combined with another dimer ($\alpha_1\beta_1$) to give the $\alpha_2\beta_1\gamma_1$ tetramer. Neither HbF or its mixed hybrid tetramer $\alpha_2\beta_1\gamma_1$ can enter the HbS polymer phase (53). Even if the β -subunit in the mixed hybrid tetramer enter the aggregation of the HbF, the polymerization in this end could be terminated because the consecutive γ -subunit is an inactive site that does not interact with other HbS. Thus, the γ -subunits are hydrophilic both with respect to cytosol and β -subunits. We will investigate the inhibitory effect at different HbF levels in future studies.

Simulations were carried out at the Argonne Leadership Computing Facility through the Innovative and Novel Computational Impact on Theory and Experiment program at Argonne National Laboratory.

The work described in this article was supported by National Institutes of Health grant No. R01HL094270 and National Science Foundation grant No. CBET-0852948.

REFERENCES

- Lee, C. C., C. Grenier, ..., A. P. Schenning. 2009. Preparation and characterization of helical self-assembled nanofibers. *Chem. Soc. Rev.* 38: 671–683.
- Spector, M., A. Singh, ..., J. Schnur. 2001. Chiral self-assembly of nanotubes and ribbons from phospholipid mixtures. *Nano Lett.* 1: 375–378.
- Ziserman, L., A. Mor, ..., D. Danino. 2011. Curvature instability in a chiral amphiphile self-assembly. *Phys. Rev. Lett.* 106:238105.
- Ross, C. A., and M. A. Poirier. 2004. Protein aggregation and neurodegenerative disease. *Nat. Med.* 10 (Suppl):S10–S17.
- Noguchi, C. T., and A. N. Schechter. 1985. Sickle hemoglobin polymerization in solution and in cells. *Annu. Rev. Biophys. Biophys. Chem.* 14:239–263.
- Admirand, W. H., and D. M. Small. 1968. The physicochemical basis of cholesterol gallstone formation in man. *J. Clin. Invest.* 47:1043–1052.
- Pauling, L., H. A. Itano, ..., I. C. Wells. 1949. Sickle cell anemia a molecular disease. *Science.* 110:543–548.
- Mickols, W., M. F. Maestre, ..., S. H. Embury. 1985. Visualization of oriented hemoglobin S in individual erythrocytes by differential extinction of polarized light. *Proc. Natl. Acad. Sci. USA.* 82:6527–6531.
- Samuel, R. E., E. D. Salmon, and R. W. Briehl. 1990. Nucleation and growth of fibers and gel formation in sickle cell hemoglobin. *Nature.* 345:833–835.
- Stuart, M. J., and R. L. Nagel. 2004. Sickle-cell disease. *Lancet.* 364:1343–1360.
- Hofrichter, J., P. D. Ross, and W. A. Eaton. 1974. Kinetics and mechanism of deoxyhemoglobin S gelation: a new approach to understanding sickle cell disease. *Proc. Natl. Acad. Sci. USA.* 71:4864–4868.
- Noguchi, C. T., and A. N. Schechter. 1981. The intracellular polymerization of sickle hemoglobin and its relevance to sickle cell disease. *Blood.* 58:1057–1068.
- Vekilov, P. G. 2007. Sickle-cell hemoglobin polymerization: is it the primary pathogenic event of sickle-cell anaemia? *Br. J. Haematol.* 139:173–184.
- Ferrone, F. A., J. Hofrichter, and W. A. Eaton. 1985. Kinetics of sickle hemoglobin polymerization. II. A double nucleation mechanism. *J. Mol. Biol.* 183:611–631.
- Eaton, W. A. 2003. Linus Pauling and sickle cell disease. *Biophys. Chem.* 100:109–116.
- Ferrone, F. A. 2004. Polymerization and sickle cell disease: a molecular view. *Microcirculation.* 11:115–128.
- ten Wolde, P. R., and D. Frenkel. 1997. Enhancement of protein crystal nucleation by critical density fluctuations. *Science.* 277:1975–1978.
- Shiryayev, A., and J. D. Gunton. 2004. Crystal nucleation for a model of globular proteins. *J. Chem. Phys.* 120:8318–8326.
- Lutsko, J. F., and G. Nicolis. 2006. Theoretical evidence for a dense fluid precursor to crystallization. *Phys. Rev. Lett.* 96:046102.
- Turner, M. S., R. W. Briehl, ..., R. Josephs. 2003. Twisted protein aggregates and disease: the stability of sickle hemoglobin fibers. *Phys. Rev. Lett.* 90:128103.
- Yang, Y. S., R. B. Meyer, and M. F. Hagan. 2010. Self-limited self-assembly of chiral filaments. *Phys. Rev. Lett.* 104:258102.
- Li, H., and G. Lykotrafitis. 2011. A coarse-grain molecular dynamics model for sickle hemoglobin fibers. *J. Mech. Behav. Biomed. Mater.* 4:162–173.
- Lei, H., and G. E. Karniadakis. 2012. Quantifying the rheological and hemodynamic characteristics of sickle cell anemia. *Biophys. J.* 102: 185–194.
- Horiuchi, K., J. Ohata, ..., T. Asakura. 1990. Morphologic studies of sickle erythrocytes by image analysis. *J. Lab. Clin. Med.* 115:613–620.
- Asakura, T., J. A. Mattiello, ..., K. Ohene-Frempong. 1994. Partially oxygenated sickled cells: sickle-shaped red cells found in circulating blood of patients with sickle cell disease. *Proc. Natl. Acad. Sci. USA.* 91:12589–12593.
- Hoogerbrugge, P. J., and J. M. V. A. Koelman. 1992. Simulating microscopic hydrodynamic phenomena with dissipative particle dynamics. *Europhys. Lett.* 19:155–160.
- Bunn, H. F. 1997. Pathogenesis and treatment of sickle cell disease. *N. Engl. J. Med.* 337:762–769.
- Dykes, G. W., R. H. Crepeau, and S. J. Edelstein. 1979. Three-dimensional reconstruction of the 14-filament fibers of hemoglobin S. *J. Mol. Biol.* 130:451–472.
- Espanol, P., and P. Warren. 1995. Statistical mechanics of dissipative particle dynamics. *Europhys. Lett.* 30:191–196.
- Grest, G. S., and K. Kremer. 1986. Molecular dynamics simulation for polymers in the presence of a heat bath. *Phys. Rev. A.* 33:3628–3631.

31. Hsieh, C.-C., S. Jain, and R. G. Larson. 2006. Brownian dynamics simulations with stiff finitely extensible nonlinear elastic-Fraenkel springs as approximations to rods in bead-rod models. *J. Chem. Phys.* 124:044911.
32. Venturoli, M., B. Smit, and M. M. Sperotto. 2005. Simulation studies of protein-induced bilayer deformations, and lipid-induced protein tilting, on a mesoscopic model for lipid bilayers with embedded proteins. *Biophys. J.* 88:1778–1798.
33. Li, X. J., I. V. Pivkin, ..., G. E. Karniadakis. 2009. Shape transformations of membrane vesicles from amphiphilic triblock copolymers: a dissipative particle dynamics simulation study. *Macromolecules.* 42:3195–3200.
34. Laradji, M., and P. B. Sunil Kumar. 2004. Dynamics of domain growth in self-assembled fluid vesicles. *Phys. Rev. Lett.* 93:198105.
35. Yamamoto, S., Y. Maruyama, and S. Hyodo. 2002. Dissipative particle dynamics study of spontaneous vesicle formation of amphiphilic molecules. *J. Chem. Phys.* 116:5842–5849.
36. Kong, Y., C. W. Manke, ..., A. G. Schlijper. 1997. Effect of solvent quality on the conformation and relaxation of polymers via dissipative particle dynamics. *J. Chem. Phys.* 107:592–602.
37. Bates, F. S. 1991. Polymer-polymer phase behavior. *Science.* 251: 898–905.
38. Huh, J., W. H. Jo, and G. ten Brinke. 2002. Conformational analysis in ABA triblock melts by Monte Carlo simulation. *Macromolecules.* 93:2413–2416.
39. Mackie, A. D., A. Z. Panagiotopoulos, and I. Szleifer. 1997. Aggregation behavior of a lattice model for amphiphiles. *Langmuir.* 13:5022–5031.
40. Horsch, M. A., Z. L. Zhang, and S. C. Glotzer. 2006. Self-assembly of laterally-tethered nanorods. *Nano Lett.* 6:2406–2413.
41. Wu, Y. Y., G. S. Cheng, ..., G. D. Stucky. 2004. Composite mesostructures by nano-confinement. *Nat. Mater.* 3:816–822.
42. Yu, B., P. C. Sun, ..., A. C. Shi. 2006. Confinement-induced novel morphologies of block copolymers. *Phys. Rev. Lett.* 96:138306.
43. Chen, P., and H. J. Liang. 2007. Origin of microstructures from confined asymmetric diblock copolymers. *Macromolecules.* 40:7329–7335.
44. Fedosov, D. A., B. Caswell, and G. E. Karniadakis. 2010. A multiscale red blood cell model with accurate mechanics, rheology, and dynamics. *Biophys. J.* 98:2215–2225.
45. Li, J., M. Dao, ..., S. Suresh. 2005. Spectrin-level modeling of the cytoskeleton and optical tweezers stretching of the erythrocyte. *Biophys. J.* 88:3707–3719.
46. Suresh, S., J. Spatz, ..., T. Seufferlein. 2005. Connections between single-cell biomechanics and human disease states: gastrointestinal cancer and malaria. *Acta Biomater.* 1:15–30.
47. Fedosov, D. A., H. Lei, ..., G. E. Karniadakis. 2011. Multiscale modeling of red blood cell mechanics and blood flow in malaria. *PLoS Comput. Biol.* 7:e1002270.
48. Pivkin, I. V., and G. E. Karniadakis. 2008. Accurate coarse-grained modeling of red blood cells. *Phys. Rev. Lett.* 101:118105.
49. Chi, P., Z. Wang, ..., A. C. Shi. 2011. Soft confinement-induced morphologies of diblock copolymers. *Langmuir.* 27:11683–11689.
50. Le Floch-Yin, F. T. 2010. Design of a numerical model for simulation of blood microcirculation and study of sickle cell disease. PhD thesis, Massachusetts Institute of Technology, Cambridge, MA.
51. Lei, H., and G. E. Karniadakis. 2012. Predicting the morphology of sickle red blood cells using coarse-grained models of intracellular aligned hemoglobin polymers. *Soft Matter.* 8:4507–4516.
52. Nagel, R. L., R. M. Bookchin, ..., K. Matsutomo. 1979. Structural bases of the inhibitory effects of hemoglobin F and hemoglobin A2 on the polymerization of hemoglobin S. *Proc. Natl. Acad. Sci. USA.* 76:670–672.
53. Akinsheye, I., A. Alsultan, ..., M. H. Steinberg. 2011. Fetal hemoglobin in sickle cell anemia. *Blood.* 118:19–27.